BIOCYBERNETICS AND BIOMEDICAL ENGINEERING 42 (2022) 391–403

Available at www.sciencedirect.com

ScienceDirect

journal homepage: www.elsevier.com/locate/bbe

Original Research Article

An iris segmentation using harmony search algorithm and fast circle fitting with blob detection

Kamil Malinowski [a,*], *Khalid Saeed* [a,b]

[a] *Faculty of Computer Science, Bialystok University of Technology, Bialystok, Poland*
[b] *Department of Computer Science and Electronics Universidad de la Costa - CUC, Barranquilla, Colombia*

ARTICLE INFO

Article history:
Received 21 July 2021
Received in revised form
15 February 2022
Accepted 22 February 2022
Available online 4 March 2022

Keywords:
Eye pupil
Iris segmentation
Eye noise
Imperfection
Blob detection

ABSTRACT

Pupil and iris segmentation based on ellipsis or circle recognition are sensitive to light reflections and reflected images. The method presented here is independent of size and shape and at the same time insensitive to light reflections and reflected mirror images. The pupil detected using the algorithm can be a reference point to further segmentation of the sclera of the eye as well as of the iris. The method is also effective when the pupil and iris are not positioned perpendicularly to the camera eye. The algorithm's average segmentation accuracy for all tested databases was 96% when considering only noisy and distorted images whilst a result of 100% was achieved with unblurred and clear images. The proposed method can be quickly and simply reproduced with a combination of known image processing methods. The developed algorithm for detecting the eyelid boundaries is effective with noisy and poor quality images due to the use of edge approximation using the Harmony Search Algorithm. An optimized shape detection method was used to detect the pupil and its edges. A method based on the variation and the average was used to eliminate shadows and eyelashes. The proposed scheme was tested on the UBIRIS.v1 database, MMU.v1 database and MILES databases, providing high results and short segmentation time. Segmentation accuracy for UBIRIS.v1 was 98.14%, for MMU.v1 – 90% and for MILES – 99.8%.

1. Introduction

Biometrics is a technique for measuring all living things. Biometric techniques are one of the fastest growing fields of IT. In its latest applications it is focused on identifying and recognizing users based on their characteristics. Biometrics is used as a method of access control, user authorization and work time recording. The use of biometrics reduces the time of identification and authorization. An example of a system that can identify and authorize people is the iris recognition system, and the solution presented in this publication is one of the many iris segmentation patterns available. The algorithm

* Corresponding author at: Faculty of Computer Science, Bialystok University of Technology, ul. Wiejska 45A, 15-351 Białystok, Poland. E-mail address: k.malinowski@doktoranci.pb.edu.pl (K. Malinowski).
https://doi.org/10.1016/j.bbe.2022.02.010

developed by us can be easily implemented, and the method of user authentication based on the iris guarantees its high stability and repeatability. The development of biometrics is particularly visible in banking, where it is used to authorize users as one of the authentication stages. The presented segmentation method can be used in medicine as one of the stages of detecting early disease symptoms of the pupil or iris, which proves its universality. The developed method may be helpful in such diseases as Cycloplegia [1]. Another important application of the method may be the location of the pupil for macular pathology studies [2]. The pupil area detected using our method is independent of its size. The experimental images had pupils of different sizes - the exact determination of the pupil area may be helpful in the analysis of lesions.

We demonstrate that the proposed method ensures excellent efficiency in the segmentation process. The use of HSA for the approximation of the eyelid boundaries gave satisfactory results. The method of detecting the inner border of the iris, developed by us, allows detection of the border of the pupil with high accuracy, even if the pupil does not have the shape of a circle due to imperfections of the recorded image or disease. The pupil detection and segmentation algorithm is yet another way to use the shape and color detector. The solution proposed in this publication was tested on UBIRIS.v1 database [3], MMU.v1 database [4], MILES [5].

It is worth noting that human identification and authorization can be carried out on other structures of the human eye. Publications presenting the process of segmentation and user recognition based on the retina of the human eye constitute a good example of it.

Iris segmentation algorithms developed over the last few years are characterized by high precision. Unfortunately, the methods using machine learning used for this purpose require time-consuming training. On the other hand, those using classical image processing are either difficult to implement or have been tested on only one set of images. What is more, some of the segmentation algorithms were tested by the authors on only one database, which does not make the research complete.

The question of the availability and simplicity of the implementation of iris segmentation algorithms should be considered. Our task was to develop a simple and quick system of the eye structures segmentation for pupil and iris, and to check whether the created system meets the standards and requirements for human recognition systems. For this purpose, we used modified, readily available algorithms to achieve high precision of operation. We compared the method developed by us to four selected works discussed in this publication, obtaining better results in the process of iris segmentation.

2. State of the art

Sundaram et al. [6] chose as the goal of their work the formulation of a hybrid segmentation algorithm solely for the extraction of blood vessels from the fundus image. The proposed algorithm uses morphological operations and a multiscale vascular strengthening algorithm. After executing the proposed algorithm, the authors use an area morphological operator to highlight the blood vessels, which is a novel mask generation scheme to extract the retinal vascular system from the fundus images.

Sadikoglu et al. [7] developed a user recognition system by means of a neural network consisting of 32 neurons and the eye's retina. The paper describes all stages, from the acquisition of the retina of the eye to the extraction of features and recognition. The system was implemented in the MATLAB environment, achieving a recognition precision of 97.5%. Unfortunately, the authors tested their method only on one database. In the discussed study, the authors did not provide the FAR, FRR, EER coefficients for the system they developed.

Meng et al. [8] in their work focused on solving the problem of deformation of the recorded image of the retina. In order to solve the above problem, the authors proposed a method of image preprocessing based on the Improved Circular GaborTransform (ICGF). The use of ICGF resulted in a reduction in the number of non-information Scale Invariant Feature Transform (SIFT) key points used for retinal-based identification. The EER of the method presented is not greater than 0.0065.

Borah et al. [9] proposed a biometric system for human recognition using two inputs: fingerprint and eye retina. The method uses artificial neural networks. The authors declare that their verification system is effective at 94.5% for the retina and 95.2% for fingerprints.

Ortega et al. [10] presents another way of using the eye's retina for the purpose of human authentication. The method developed by the authors is similar to that used for fingerprints. In order to obtain key points, an algorithm based on folds is used in the user verification process. The characteristics of the points selected in this way are retrieved recursively by tracing the folds from the located optical disk. The authors declare that their system has reached the EER 0%.

Abdelwahed et al. [11] achieved a segmentation precision of 99.12% using the segmentation algorithm developed on the basis of UBIRIS.v1 database [3]. Daugman's Integro-Differential and edge-based techniques were used in the work.

Rapaka et al. [12] used morphological reconstruction fuzzy c-means clustering based on an improved differential search algorithm. The authors estimated the efficiency of the method at 95.27%. Unfortunately, no pupil segmentation was done, as they focused solely on the iris of the eye. UBIRIS.v1 database [3], along other sources, was used during testing.

Varkarakis et al. [13] based their algorithm on Deep Neural Networks. Despite the low complexity of the proposed method, they achieved high level of accuracy of the iris segmentation. A camera installed in virtual reality glasses was used to obtain the data.

Jan et al. [14] used an optimized coarse-to-fine scheme based on an adaptive threshold in order to define the inner and outer boundaries of the iris. Then, using the Fourier series, they precisely delineated the border of the iris.

Hao et al. [15] used feature channel optimization for noisy image to solve the problem of iris segmentation. Their proposed solution was based on Jensen-Shannon divergence.

Sahmoud et al. [16] analyse the colour information for different colour spaces (RGB, YCbCr, and HSV) in order to select a suitable iris for further segmentation.

Other approach to solving the problem of pupil segmentation [17] is application of colour mapping algorithm. Authors claim the effectiveness of their solution to be at 98%.

Lee et al. [18] estimate the pupil centre using orientation fields, followed by edge detection using a gradient. Then an approximate radius based on the circular histogram of the detected pupil edges is established. Unfortunately, the algorithm will work only if the entire iris is clearly visible in the image and the pupil is similar to the circle or ellipse.

Omran et al. [19], to localize the pupil, authors enhance the image by using histogram equalization and median filter. Gamma correction and blurring disk filter is used to determine the pupil boundary.

ŞIMŞEK et al. [20] used a modified Wildes algorithm to solve the problem of pupil segmentation. In order to detect pupil edges they created a method free from the issue of mirror points reflections. It consists of a morphological filter and a two-way scanning method. Eyelids are detected using the Refine-Connect-Extend-Smooth (R-C-E-S). The authors did not test the algorithm for images recorded in visible light spectrum.

Jalilian et al. [21] developed an algorithm that does not require additional information to estimate the angle under which the photo of the human eye was taken. The developed algorithm is based on the measurement of the relative distance of empirically determined characteristic points of the iris and the pupil. Based on the above procedure, input segmentation masks for CCN are generated. The obtained information enables the correction algorithm (KKN classifier, ellipse adjustment, differential operator) to estimate the area of the iris. According to the authors, the algorithm was 97% effective. Unfortunately, the authors tested the developed solution on one database.

Jan et al. [22] used bilinear interpolation and a statistical filter to remove noise visible as light reflexes in the image. The pupil of the iris is determined by extracting the largest circular area after applying image binarization. The outer boundary of the iris, on the other hand, is determined using the Circular Hough Transform (CHT). The final step is to use the Fourier series to accurately define the boundaries of the iris of the eye. The method is sensitive to noise and imperfections of images. The authors tested their algorithm only on infrared images.

Sardar et al. [23] used the Interactive Squeeze Expand UNet (ISqEUNet) method developed by them to solve the problem of iris segmentation. The proposed method is an extension of the method using the convolutional neural network (CNN) architecture by implementing a squeeze layer with 1×1 convolution layer. The algorithm uses interaction with the user to detect the iris more efficiently for noisy and imperfect images. The method was tested in an efficient and expensive environment (Nvidia Quadro K6000 GPU with 12 GB DDR5 RAM) reaching an average segmentation time of 9.106e-06 sec.

Jan et al. [24] after predefining a circular region containing the iris of the eye apply an iterative scheme involving Hough transform to segment the iris. The final segmentation step is based on the use of Lagrange interpolating polynomial to accurately define the contours of the iris. The algorithm has been tested only on infrared images.

Li et al. [25] used the Faster R-CNN model to correctly detect the position of the human eye. The outer boundary and the inner iris are detected using the pretrained Gaussian mixture model, maximization of the intensity gradient along the radial emitting path and boundary point selection algorithms. The algorithm was tested on a single database of infrared images. The authors declare the effectiveness of the method at the level of 95.49% with an average execution time of 0.06 sec.

3. Proposed iris segmentation

First step is to remove dust, scratches and undesirable objects, applied blur to the image using a Gaussian filter. Then we reconstruct the image from the pixel near the area boundary to eliminate light reflections in the pupil. The procedure described above guarantees correct detection of the eye pupil in the subsequent stages.

In order to segment the pupil, the image is subjected to thresholding procedure. This way, several images are obtained which differ in brightness threshold value. In each of the images thus segmented groups of points are found, for which mass centres are calculated. Then, groups of points on all images are merged when their mass centres are apart by less than previously established and set value. Detected white spots are analysed for shape so that only those satisfying the conditions are selected:

- roundness [26,27] (1)

$$O = \frac{4\pi * area\ of\ analysed\ element}{perimeter^2} \tag{1}$$

- convexity [26,27] (2)

$$W = \frac{\text{area of analysed element}}{\text{convex hull area of analysed element}} \tag{2}$$

- inertia coefficient - inertial resistance of the object to rotation around its main axes [26,27] (3)

$$W_b = \frac{I_{min}}{I_{max}} \tag{3}$$

where,

$$I = \frac{1}{2}(c+a) - \frac{1}{2}(a-c)cos2\theta - \frac{1}{2}bsin2\theta$$

$$cos2\theta = \frac{\pm(a-c)}{\sqrt{b^2+(a-c)^2}}, sin2\theta = \frac{\pm b}{\sqrt{b^2+(a-c)^2}}$$

$$a = m_{20} - \frac{m_{10}^2}{m_{00}}, b = m_{11} - \frac{m_{10} * m_{01}}{m_{00}}, c = m_{02} - \frac{m_{01}^2}{m_{00}}$$

$(x_1, y_1), \cdots, (x_N, y_N)$
– *points belonging to the contour of the tested object*

$$a_{00} = \sum_{i=1}^{N} x_N * y_i - x_i * y_N$$

$$a_{10} = \sum_{i=1}^{N} (x_N * y_i - x_i * y_N) * (x_N + x_i)$$

$$a_{01} = \sum_{i=1}^{N} (x_N * y_i - x_i * y_N) * (y_N + y_i)$$

$$a_{11} = \sum_{i=1}^{N} (x_N * y_i - x_i * y_N) * (x_N * (2y_N + y_i) + x_i * (2y_i + y_N))$$

$$a_{20} = \sum_{i=1}^{N} (x_N * y_i - x_i * y_N) * (x_N * (x_N + x_i) + x_i^2)$$

$$a_{02} = \sum_{i=1}^{N} (x_N * y_i - x_i * y_N) * (y_N * (y_N + y_i) + y_i^2)$$

$$m_{00} = \pm\frac{a_{00}}{2}, m_{10} = \pm\frac{a_{10}}{6}$$

$$m_{01} = \pm\frac{a_{01}}{6}, m_{11} = \pm\frac{a_{11}}{24}, m_{20} = \pm\frac{a_{20}}{12}, m_{02} = \pm\frac{a_{02}}{12}$$

From the above equation (3) [26,27] we choose positive solution for I_{min} and negative solutions for I_{max}. Result of equation (3) [26,27] close to 0 means that the tested object is a line, while the value close to 1 means that the tested object is a circle. If b = 0 and a = c then object is rotationally symmetric. In the next stage, morphological operators and binarization were used using the Minkowski sum and difference respectively [28].

The final stage of the method is to define the boundaries of the detected pupil. Here, the boundary detection algorithm described in detail in publication [29] was used. The points constituting the detected boundary are initial elements for convex hull search algorithm [30] and circumscribe a circle which completely covers the object with minimum area. The average value of colour in these two designated areas is calculated. The area of the pupil with the lower value is considered to be the correctly determined one. The final result of the search for the pupil of the eye is shown in Fig. 1 and Fig. 2.

The flow chart of the proposed pupil detection is shown in Fig. 3.

The next step is to binarize the whole image using the Otsu method [31] and to smooth it using Gaussian filter, because we need the accurate gradient director in next step. The largest black area is then selected for the next step in eye segmentation.

The outer border of the iris should be searched for in the range from R_{min} = 50 to R_{max} = 150. These values were used for all images and are independent of the image. Prior to R value search procedure images from UBIRIS database v1 [3] and MILES Iris Dataset [5] have been reduced to the size of 240x340 pixels, whereas the images from the MMU.v1 [4] database are natively in the size of 240x340 pixels. These values were expanded experimentally after analyzing all images from the selected

Fig. 1 – The extracted pupil area from the input image.

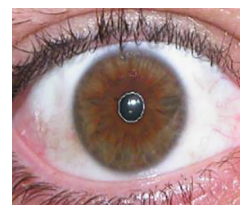

Fig. 2 – Determined eye pupil boundary superimposed on the input image.

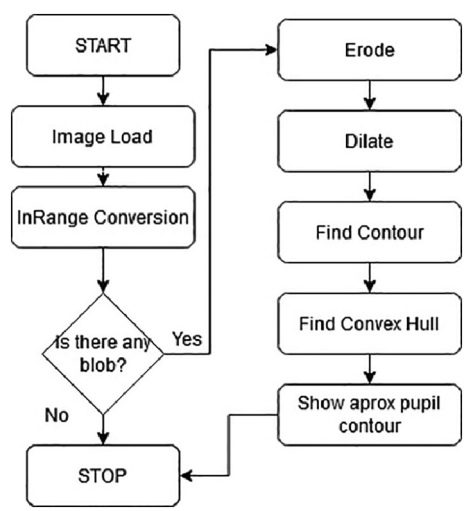

Fig. 3 – Flow chart of the proposed pupil detection.

databases. Determining the points belonging to the outer border of the iris can be described in the following stages:

Step 1: calculate the intensity gradients values at edge pixels using the Sobel operator [32] (4):

$$g = (g_x^2 + g_y^2)^{\frac{1}{2}} \tag{4}$$

g_x – image gradient X axis.
g_y – image gradient Y axis.
g, g_x, g_y are column vectors.

Step 2: generate stroke pixels (x_c, y_c) [32] (5):

$$x_c = x - R\left(\frac{g_x}{g}\right) \tag{5}$$

$$y_c = y - R\left(\frac{g_y}{g}\right)$$

R – row vector with values $< R_{min}, R_{min} + 0.5n, \ldots, R_{max} >$ n = 1,2,3. . ., (R_{max}-R_{min})/0.5.
(x, y) – coordinates of points belonging to the detected edges.

Step 3: detect a range of radii of circles by using phase code for radius - the log phase coding [33] (6).

$$C = \frac{e^{i\varphi_R}}{R}$$

$$\varphi_R = 2\pi\left(\frac{logR - logR_{min}}{logR_{max} - logR_{min}}\right) \tag{6}$$

Step 4: find local (regional) maxima in *H* – circle center [34], H contains the elements of the array filled with C indices with values taken from the vector [x_c, y_c]. The repetition of the indexes causes the accumulation of values.

Step 5: calculate the circle radius - undo the phase coding (7).

$$r = e^{\frac{H_{xy}}{2\pi}(logR_{max} - logR_{min})} + logR_{min} \tag{7}$$

$$ifH_{xy} < 0, H_{xy} = 2\pi$$

H_{xy} – coordinates X of circle center (maxima in H).

Step 6: select all the points that satisfy the inequality (8).

$$0.8r \le (x, y) \le 1.2r \tag{8}$$

Fig. 4 shows the effect of the abovementioned steps.

The previously detected points are the reference points for the circle fitting algorithm. There are several known algorithms that allow you to adjust the circle from noisy points. In order to precisely define the boundaries of the iris of the eye, the circle fitting algorithm developed by Al-Sharadqah and Chernov was used [35], which is numerically superior to all previously known algorithms.

Consider the circle described as follows (9):

$$E(x_i^2 + y_i^2) + Bx_i + Cy_i + D = 0 \tag{9}$$

The problem of circle fitting is reduced to the minimization of the function (10):

$$F(A, \eta) = A^T MA - \eta(A^T NA - 1) \tag{10}$$

where η is Lagrange multiplier and A = (E, B, C, D) is the vector of the parameters from equation (9).

At the same time, equation (10) can be reduced to solve the general problem of minimizing the value of η (11):

$$\text{lack } (M - \eta N)A = 0$$

where:

$$Z = \begin{bmatrix} x_1^2 + y_1^2 & x_1 & y_1 & 1 \\ \vdots & \vdots & \vdots & \vdots \\ x_n^2 + y_n^2 & x_n & y_n & 1 \end{bmatrix}$$

$$M = \frac{1}{n} Z^T Z$$

$$N = \begin{bmatrix} 8\bar{z} & 4\bar{x} & 4\bar{y} & 2 \\ 4\bar{x} & 1 & 0 & 0 \\ 4\bar{y} & 0 & 1 & 0 \\ 2 & 0 & 0 & 0 \end{bmatrix} \tag{11}$$

$$\bar{x} = \frac{1}{N}\sum x_i, \bar{y} = \frac{1}{N}\sum y_i, \bar{z} = \frac{1}{N}\sum x_i^2 + y_i^2 \tag{12}$$

Fig. 5 shows the effect of the algorithm described above.

The highly noisy image of the iris of the human eye is obscured by the upper and lower eyelids. The edge of the eyelid is an area darker than the surrounding area.

The common and effectives methods to filter out the eyelid are based on parabolic models and edge detection techniques [36,37].

Therefore, the method of segmentation of the area covered by the eyelids is proposed below.

The previously defined area of the eye after is divided into two parts, as shown in Fig. 6.

The area under and above the centre of the pupil line is searched in parallel along the points constituting the line Y1 and Y2 to find eyelid point. We find the minimum value where the ratio of values greater than 128 to values lower than 128 towards the pupil centre is the smallest; the point is classified as the region of eyelid boundary - otherwise eyelid is not found. The above operation minimizes the area of the eyelid edge search, false positive point and increases its effectiveness. Points with the lowest value for each column of the image are extracted from the designated areas along the horizontal. Fig. 7 shows the final result.

The points obtained in this way are the input data for the curve approximation algorithm. In our work, we used a curve approximation algorithm using a second degree polynomial to find points belonging to near eyelid.

The edge representing the eyelid can be shown through the following function (13):

$$F(x) = Ax^2 + Bx + C \tag{13}$$

Factor A has positive values for the lower eyelid points and negative values for upper eyelid points. With three random given points, that is P_1=(x_1,y_1), P_2=(x_2,y_2), P_3=(x_3,y_3) the solution (equation of the corresponding parabola) comes down to solving three linear equations (14).

$$y_1 = Ax_1^2 + Bx_1 + C$$

$$y_2 = Ax_2^2 + Bx_2 + C \tag{14}$$

$$y_3 = Ax_3^2 + Bx_3 + C$$

Fig. 4 – Effect of edge filtering algorithm.

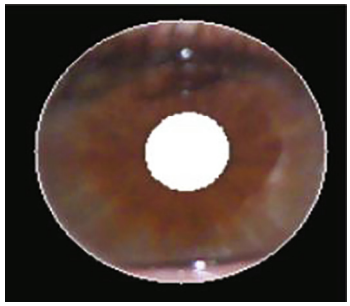

Fig. 5 – Approximate area of the iris of the eye.

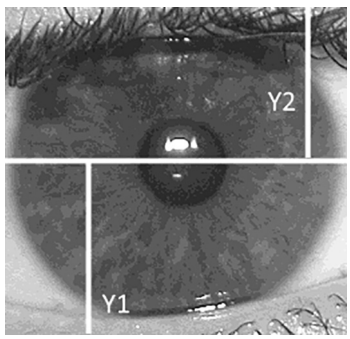

Fig. 6 – Division of the iris of the eye before the separation of the areas covered by the eyelids.

This corresponds with the following matrix notation (15):

$$\begin{Bmatrix} x_1^2 & x_1 & 1 \\ x_2^2 & x_2 & 1 \\ x_3^2 & x_3 & 1 \end{Bmatrix} \begin{Bmatrix} A \\ B \\ C \end{Bmatrix} = \begin{Bmatrix} y_1 \\ y_2 \\ y_3 \end{Bmatrix} \tag{15}$$

The above matrix can be solved symbolically avoiding unnecessary and complicated matrix calculations using Cramer's rule (16):

$$\begin{aligned} A &= \frac{y_1(x_2-x_3)+y_2(x_3-x_1)+y_3(x_1-x_2)}{(x_1-x_3)(x_2-x_3)(x_1-x_2)} \\ B &= \frac{y_1\left(x_3^2-x_2^2\right)+y_2\left(x_1^2-x_3^2\right)+y_3\left(x_2^2-x_1^2\right)}{(x_1-x_3)(x_2-x_3)(x_1-x_2)} \\ C &= \frac{y_1\left(x_2^2x_3-x_3^2x_2\right)+y_2\left(x_3^2x_1-x_1^2x_3\right)+y_3\left(x_1^2x_2-x_2^2x_1\right)}{(x_1-x_3)(x_2-x_3)(x_1-x_2)} \end{aligned} \tag{16}$$

The above procedure should be performed for all possible combinations of the three points, independently for the upper and lower eyelids. The parabolas with the most matching points are selected for the border of the eyelids (one for the upper and lower eyelids).

The problem of qualifying the points belonging to the eyelid edge (parabola) comes down to minimising the function (17):

$$J(S) = 1 - \frac{\sum_{c=1}^{N} E(x_c, y_c)}{N}, \textit{where}$$

$$E(x_c, y_c) = \begin{cases} 1 & \textit{if point } (x_c, y_c) \textit{onthe edge} \\ 0 & \textit{otherwise} \end{cases} \tag{17}$$

There are numerous methods to solve the problem of minimising the function. In our work, we used the Harmony Search Algorithm (HSA) method developed by Geem et al. [38]. Harmony Search Algorithm is classified as an evolutionary algorithm. The algorithm was inspired by the process of musicians improvising while playing instruments. During improvisation, the musicians choose the key of the tune in order to best suit the entire ensemble. The improvising musicians, after a short time of improvisation, begin to perform the piece almost perfectly. The harmonic memory used in HSA to store solutions can be compared to the population of individuals used in evolutionary algorithms. Mutation, on the other hand, takes place through improvisation, while the equivalent of crossing is the construction of a new solution based on randomly selected values from the harmonic memory. Parameters by which the process of searching for the solution space is controlled:

- BW - scope of modification of the decision variable selected from the harmonic memory;
- HMCR - the probability of using the harmonic memory to determine the value of the decision variable;
- HMS - harmonic memory size;
- NI - the maximum number of iterations of the algorithm;
- PAR - the probability of modification of a decision variable selected from the harmonic memory.

Table 1 presents the parameters of Harmony Search Algorithm used in this work for all tested databases.

The final stage of the segmentation of the iris is the removal of eyelashes and shadows. There are many algorithms for removing eyelashes and shadows. One of such ways is to remove the highest intensity points from the analysed image. Nadia et al. [39] used histogram equalization, non maximum suppression, thresholding and then eliminate noise greater than 50 pixels. Unfortunately, even though the authors declared high efficiency of the algorithm in the region of 99.99%, the algorithm was tested on one data base only.

In our work we implemented a modified algorithm proposed by Liu et al. [40]. Liu et al. [40] divide the detected area of the iris after conversion to grayscales into three non-overlapping parts of the same height. In our work, we modified the algorithm to work for difrent database than UBIRIS. v1 database [3], by dividing the area of the iris into two equal parts horizontally – line X (Fig. 8).

In order to detect whether the image of the iris is obscured by the eyelashes, the following relation should be used (18):

$$ELS = \frac{\mu_1 - \mu}{\mu_1} \tag{18}$$

where μ_1, δ – mean/standard deviation value of region just above lower eyelid, μ - mean of intensity in the region just below upper eyelid.

If the calculated *ELS* value is lower than 0.1 it means that eyelashes were detected in the analysed image. If the intensities of the analysed pixel and of more than one of its 8-neighbor are less than $\mu_1 - 2.1\delta$ at the same time, then this pixel is removed. The above 2.1 constant was deduced from

Table 1 – Parameter for the HSA detector.

HMS	HMCR	PAR	BW	NI
150	0.7	0.3	2	200

the analysis of all images from tested databases. The flow chart of the proposed iris detection is shown in Fig. 9.

4. Experimental result

Incorrect functioning of the segmentation algorithm may result in different representations of the pattern of the same iris. The development of a method for determining the exact area of the iris is the key element in effective segmentation. In order to determine the effectiveness of the proposed method, the foreground area error (RFAE) and accuracy (ACC) (19) [41] was used.

$$RFAE = \begin{cases} \frac{(TP+FN)-(FP+TP)}{TP+FN}, if(FP+TP) < (TP+FN) \\ \frac{(FP+TP)-(TP+FN)}{FP+TP}, if(FP+TP) \geq (TP+FN) \end{cases} \quad (19)$$

$$ACC = \frac{TP+TN}{TP+TN+FN+FP}$$

where TP – areas of true positive, TN – areas of true negative, FP – areas of false positive, FN – areas of false negative. The above-mentioned parameters range from 0, (meaning perfectly correct segmentation) to 1, meaning error. Each of test images was labelled to carefully construct the ground-truth segmentation for evaluating the proposed algorithm's segmentations.

Successfully segmented rate versus relative foreground area error for UBIRIS.v1 database [3], MMU.v1 database [4] and for MILES [5] for pupil, eyelid, eyelashes, iris is shown in Figs. 10, 11, 12, 13, respectively. The successful segmentation rate is defined as the ratio of the number of images with segment results achieving a threshold to the size of the all tested images from database.

The test platform was a computer equipped with Intel® Core™ i7-1135G7 processor. Table 2 shows the time complexity of the proposed method step by step.

When measuring code efficiency, a ready-made BenchmarkDotNet library was used. This library creates dedicated projects for each method on the fly to measure their performance in isolation. Measuring code performance is not an easy topic since you can make a lot of mistakes that may lead to wrong conclusions. That is why we used ready-made tools such as BenchmarkDotNet, which facilitate this process and eliminate the basic problems.

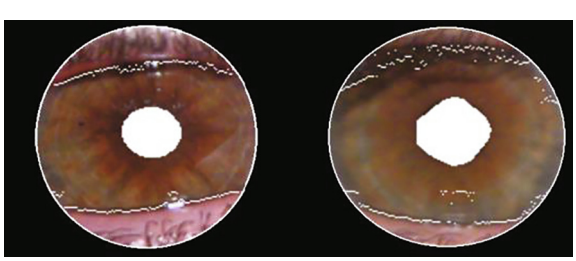

Fig. 7 – Points that are candidates for further separation of the lower and upper eyelids.

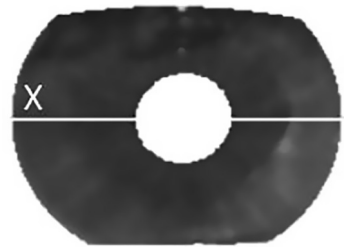

Fig. 8 – Division of the iris of the eye before the eyelashes and shadow remove.

Fig. 14 shows an example of the performance of authors' algorithm for images with low noise and imperfections.

Biometrics is often used as a replacement for standard user-entered passwords. Unfortunately, there is a fundamental difference that distinguishes the use of biometrics for user authentication compared to standard authentication methods. By entering the password, the system will authenticate us, provided that the password entered is identical to the one in the database of the authentication system. In the case of biometrics, the chance of creating identical images is small. In conclusion, checking for the perfect match of the authentication pattern in the case of biometrics would cause the system to malfunction - it would not be possible to authorize on this basis. The more restrictive the system is, the more burdensome it will be for users. Identification systems based on biometric features must have a specific error acceptability rate.

The key role is to select such parameters for the feature comparator so that the biometric system is safe and the least onerous. This can be achieved by two key indicators for authentication systems based on biometrics - FRR (False Rejection Rate) and FAR (False Acceptance Rate). The first indicator tells us how many positive results were classified as negative, while the second one indicates how many incorrect results were classified as correct. A high FRR or FAR ratio means a greater nuisance for potential user.

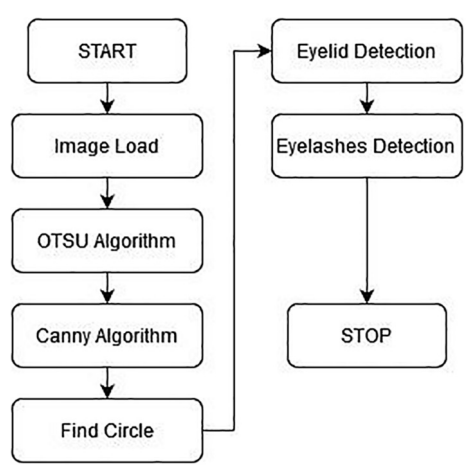

Fig. 9 – Flow chart of the proposed iris detection.

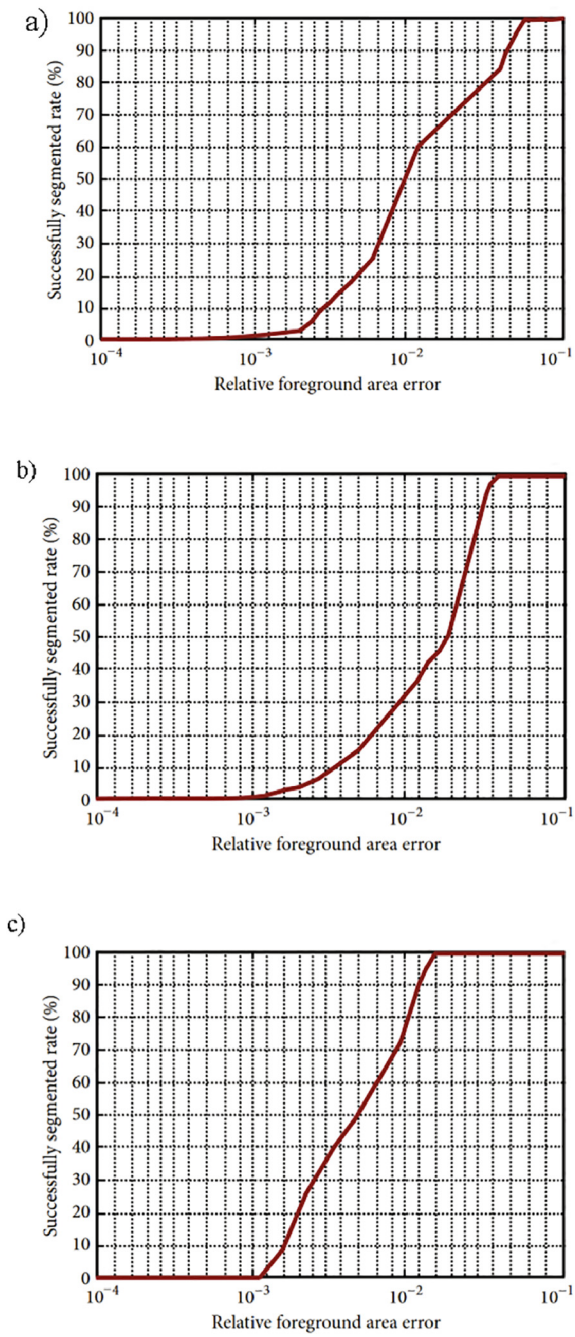

Fig. 10 – Successfully segmented rate versus relative foreground area error for pupil – a) UBIRIS.v1 database [3], b) MMU.v1 database [4], c) MILES [5].

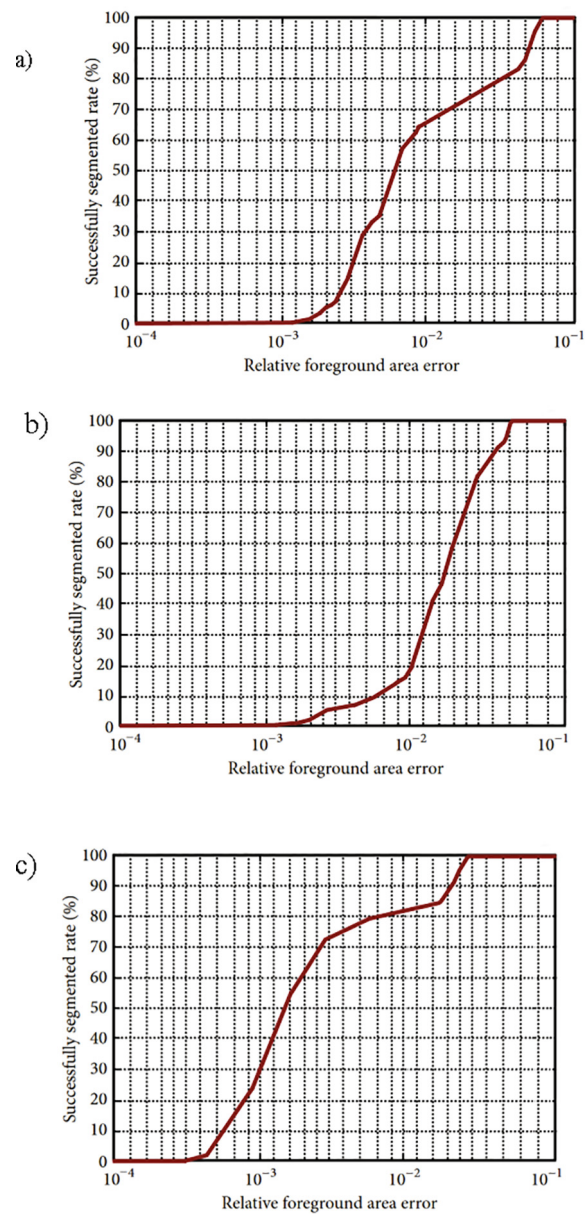

Fig. 11 – Successfully segmented rate versus relative foreground area error for eyelid – a) UBIRIS.v1 database [3], b) MMU.v1 database [4], c) MILES [5].

The EER (Equal Error Rate) should also be mentioned, as it is a compromise between the convenience and effectiveness of the biometric recognition system. The EER factor is determined using the FRR and FAR ratios discussed above. A system with a lower EER is more accurate. The EER value indicates that the proportion of false acceptances is equal to the proportion of false rejections.

In most algorithms currently in use, the structure of the iris is coded according to the Daugman algorithm. According to the Daugman algorithm, the area of the iris of the eye is decomposed using the Gabor transform. The Gabor transform finds representations of features in a complex space. The most distinguishing features are extracted by calculating the frequency values of the Gabor transform, so it divides the input signal into real and imaginary components. The correctness of the recognition algorithm operation was assessed by analysing the FRR and FAR coefficients using the Gabor and Hamming Distance transformations. After a series of experiments, it was established that the Hamming distance between the photos of less than 0.29 means that we are dealing with the irises of the same people.

In order to determine the coefficients of incorrect FRR and FAR analysis, tests of the algorithm were carried out on 300 images of irises (100 randomly selected images from each datasets - UBIRIS.v1 database [3], MMU.v1 database [4], MILES

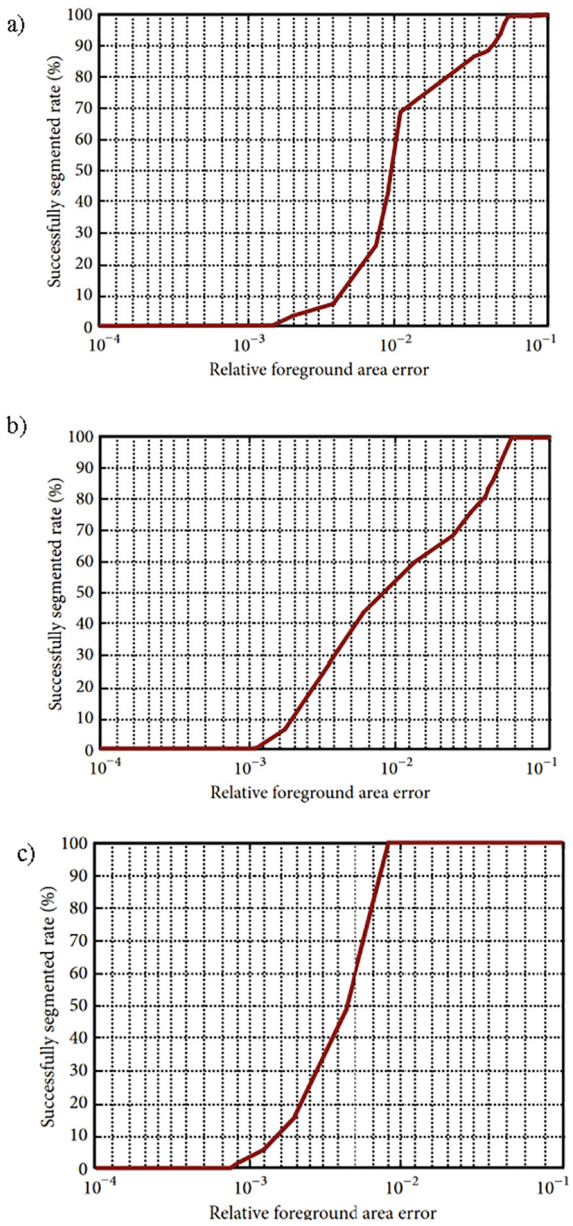

Fig. 12 – Successfully segmented rate versus relative foreground area error for iris – a) UBIRIS.v1 database [3], b) MMU.v1 database [4], c) MILES [5].

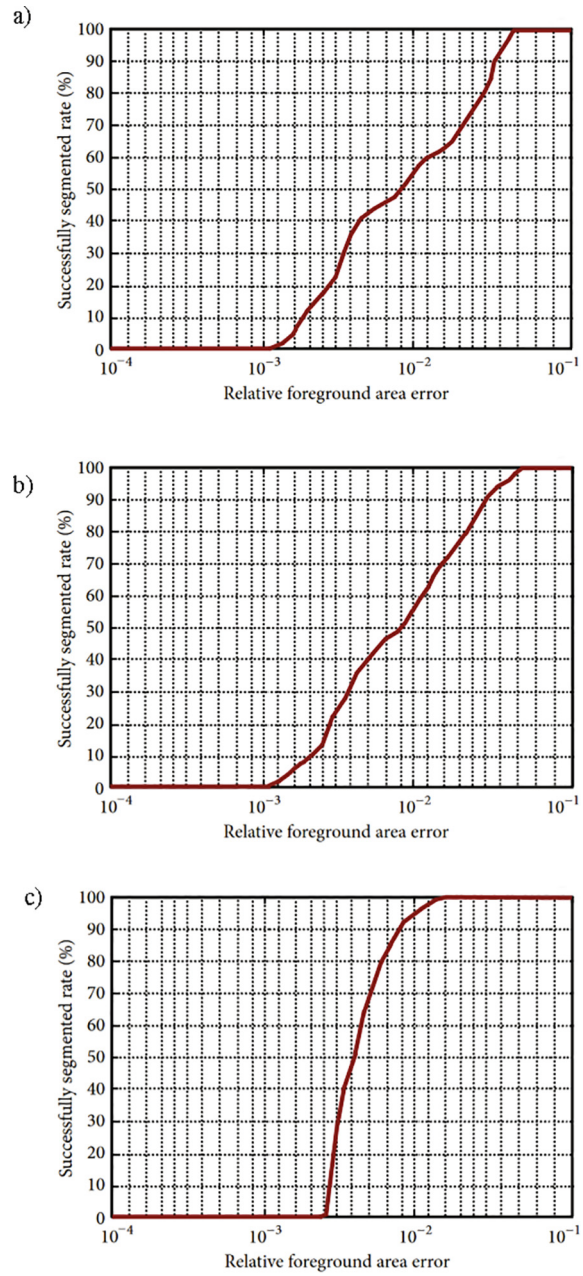

Fig. 13 – Successfully segmented rate versus relative foreground area error for eyelashes – a) UBIRIS.v1 database [3], b) MMU.v1 database [4], c) MILES [5].

Iris Dataset [5]). The images selected for the experiments do not contain undesirable elements in the form of glasses, and only images where the eyelids in the recorded image are arranged horizontally were used. The method developed by us may be improved in the future by introducing elements that eliminate the above-mentioned elements. FRR is the ratio of the false negatives to the sum of the true positive and false negative. The test allowed determining the FRR ratio at the level of 3%. The FAR coefficient for the implemented algorithm was determined at the level of 5.8%. FAR is the ratio of the false positive to the sum of the false positive and true negative.

Table 2 – Time complexity of the proposed method.

Segmentations step	Time (ms)		
	Minimum	Maximum	Average
pupil	9	47	11
eyelid	32	530	95
iris	16	62	34
eyelashes	206	1800	500
Total	**263**	**2439**	**640**

Fig. 15 shows the relation between FPR (1-TPR) as the False Positive Rate against the TPR as the True Positive Rate. TPR is the ratio of the true positive to the sum of the true positive and false negative and was determined at the level of 79%.

The EER (Equal Error Rate) coefficient for the implemented algorithm was determined at the level of 3.3%.

5. Discussion

The use of the proposed second degree curve approximation method to determine the boundaries of the lower and upper eyelids gave satisfactory results. Our system of eyelid segmentation using HSA surprised us with its accuracy and speed of execution (Table 2). The average time of algorithm execution was shorter than one second. Our use of the Harmony Search Algorithm is a different approach to the problem of delineating the boundaries of the eyelids of the eye from the methods presented in the literature review. The use of the HSA algorithm for the above-mentioned purpose has not been described so far.

A minor modification of the shape recognition algorithm by an element conditioning the use of the pupil border approximation by fitting a circle or convex envelope also gave satisfactory results, comparable with the achievements of other authors.

However, the algorithm for removing eyelashes and shadows should be modified. The method used is subject to a significant error. This requires further work and analysis in the future.

Segmentation accuracy using UBIRIS database v1 [3] 98.14%, MMU.v1 [4] 90%, MILES Iris Dataset [5] 99.8%, which is comparable to other methods described over the last few years (Table 3).

The reason for the worse iris segmentation result obtained with images from the MMU.v1 database [4] is the apparent poorer quality of the images contained in this database.

Additional evidence of the high efficiency of the method in human identification is visible in the ROC characteristic and the achieved EER of about 3.3% (Fig. 15). This means that approximately every eighth verification attempt may be wrongly qualified as either positive or negative. The methods of iris segmentation described in the introduction are characterized by a similar precision of iris segmentation (Table 3). Comparing the precision of the iris segmentation methods of other authors to the precision and the FAR, FRR, EER coefficients of our solution it can be concluded that all the methods presented in Table 3 could be used in user authentication systems based on iris biometry. In our opinion, the achieved FAR, FRR, EER coefficients are acceptable and allow us to conclude that the system developed by us meets the requirements for biometric authentication systems based on the iris of the human eye.

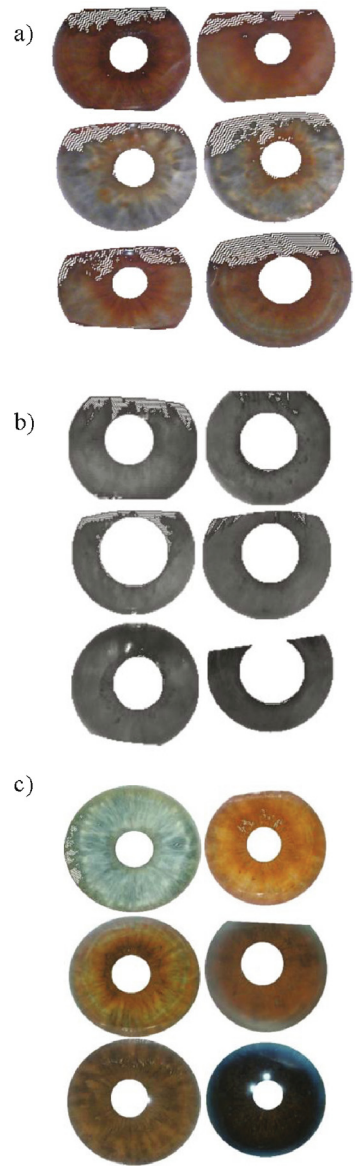

Fig. 14 – Examples of the algorithm we developed - a) UBIRIS.v1 database [3], b) MMU.v1 database [4], c) MILES [5].

Due to the very similar values of the precision of iris segmentation for the method developed by us to the method developed by Chen-Chung et al. [40] (difference 0.01%) we compared the ratio of relative foreground area error (Table 4). The algorithm developed by us performs worse with infrared

Table 3 – Comparison of accuracy of the proposed method with other known algorithms for iris segmentation.

Algorithm	Segmentation accuracy (%)		
	UBIRIS database v1 [3]	MMU.v1 [4]	MILES Iris Dataset [5]
Rapaka et al. [12]	95.27	–	–
Jan et al. [24]	–	97.97	–
Chen-Chung et al. [40]	98.13	–	–
Abdelwahed et al.[11]	99.12	–	–
Proposed method	**98.14**	**90**	**99.8**

Table 4 – Foreground area error for UBIRIS.v1 database [3], MMU.v1 database [4] and for MILES [5] for pupil, eyelid, eyelashes, iris.

Dataset	Relative foreground area error (<0.25)			
	Pupil	Eyelid	Eyelashes	Iris
UBIRIS database v1 [3]	84%	83%	87%	98%
MMU.v1 [4]	100%	97%	81%	94%
MILES Iris Dataset [5]	100%	100%	100%	100%

images, which is confirmed by the much lower accuracy than the method developed by Jan et al. [24]. The method developed by John et al [24] was not tested by its authors on images recorded in visible light.

The analysis of charts 10–13 (Table 4) allows for the following conclusions compared to Chen-Chung et al algorithm [40]:

- there are 73%, 90%, and 98% images of database UBIRIS database v1 [3] whose RFAE is no more than 0.25 after pupil and iris, eyelid, eyelashes,
- the RFAE values we achieved are better for pupil and iris segmentation and worse for eyelid and eyelashes segmentation,
- visible differences in RFAE did not deteriorate the precision of iris segmentation. In addition, our solution has been tested on more than one database.

On the other hand, taking into account the segmentation precision index of solutions proposed by Rapaka et al. [12] our method is more precise. On the other hand, taking into account the works using the retina [8,10], the method we developed yielded worse results (EER). Abdelwahed et al. [11] method has only been tested on one database. Our developed method segments the area occupied by eyelids, shadows and eyelashes, which is missing in the method developed by Abdelwahed et al. [11] which makes our algorithm more complete. Images from MILES database [5] contain less noise compared to images from UBIRIS.v1 database [3]. This ensures that better iris segmentation is obtained, which is proved in this paper. For images where the pupil area did not contain shadows or eyelashes, the algorithm we developed achieved an efficiency of 100% for images from MILES [5] and UBIRIS database v1 [3]. The problem in correct determination of iris area for images from MMU.v1 database [4] turned out to be elimination of noise caused by shadows and eyelashes, which is visible in form of the lowest value of foreground area error – 81% (Tab. 4) among all tested databases. The method of elimination of eyelashes and shadows presented in this manuscript requires further work and analysis. In addition, the authors of the MMU.v1 database [5] suggest that "*iris segmentation can be performed using segmentation based on Hough/Daugman circles or Transfer Learning*." All of the above makes it possible for the results of other algorithms to be replicated and compared with the results we achieved for MMU.v1 [4] and MILES [5]. The information in Table 4 allows us to conclude that our method can determine the pupil and iris boundaries with high accuracy.

The FRR and FAR coefficients may also be useful in medicine in detecting lesions of the iris and pupil - a case in which the system rejects user authorization attempts above a predetermined indicator may signal a disease. The HSA approximation of curves developed by us can be used to approximate blood vessels, the edges of the auricles and the skeletal system, yet it requires further work and analysis.

6. Conclusions

The implemented algorithm was tested in order to determine the FAR and FRR coefficients and the ROC characteristics. Incorrect acceptance of the iris image constitutes only 5.8% of all tests performed. The designed system FRR incorrect rejection rate is 3%. The obtained test results determining the values of the FAR and FRR coefficients are satisfactory and confirm the usefulness of the designed algorithm.

The advantage of the algorithm is that it is insensitive to pupil/iris imperfection. As one may notice, light reflections and partial obscuration of the pupil/iris by eyelashes do not hinder the proposed solution. In addition, the final result of segmentation can represent the next step in eye segmentation. To show the effectiveness of the proposed algorithm, it was tested on a various images of the human eye achieving segmentation accuracy for UBIRIS database v1 [3] – 98.14%, for MMU.v1 [4] – 90%, and for MILES Iris Dataset [5] – 99.8%.

The 96% average segmentation accuracy obtained when using the authors' algorithm was achieved without excluding any of the distorted images. However, the rate has reached 100% when considering clear images, free of noise or distortion. Our algorithm presents a procedure for solving the problem of human pupil/iris fixation based on the photos available in the three different datasets. The algorithm is simple and easy to implement in relation to the obtained efficiency. The developed algorithm is most effective when the angle at which the eye image was recorded is close to the right angle (images included in MILES Iris Dataset [5]).

Declaration of Competing Interest

The authors declare that they have no known competing financial interests or personal relationships that could have appeared to influence the work reported in this paper.

Acknowledgements

This work was supported by grant WZ/WI-IIT/4/2020 from Bialystok University of Technology and funded with resources for research by the Ministry of Science and Higher Education in Poland, and partially by CUC - Universidad de la Costa, Barranquilla, Colombia.

REFERENCES

[1] Raina UK, Gupta SK, Gupta A, Goray A, Saini V. Effect of cycloplegia on optical biometry in pediatric eyes. J Pediatr Ophthalmol Strabismus 2018;55(4):260–5.
[2] Alizadeh Y, Akbari M, Moghadam RS, Medghalchi A, Dourandeesh M, Bromandpoor F. Macular optical coherence tomography before cataract surgery. J Curr Ophthalmol 2021;33(3):317.
[3] Proença, H. and Alexandre, L.A., 2005, September. UBIRIS: A noisy iris image database. In International Conference on Image Analysis and Processing (pp. 970-977). Springer, Berlin, Heidelberg.
[4] MMU. (2013). MMU Iris Database.
[5] MILES Iris Dataset, https://drive.google.com/drive/folders/0B5OBp4zckpLnU3YxMnozSGhGelE, Accessed: 2021-06-01.
[6] Sundaram R, Ravichandran KS, Jayaraman P. Extraction of blood vessels in fundus images of retina through hybrid segmentation approach. Mathematics 2019;7(2):169.
[7] Sadikoglu F, Uzelaltinbulat S. Biometric retina identification based on neural network. Procedia Comput Sci 2016;102:26–33.
[8] Meng X, Yin Y, Yang G, Xi X. Retinal identification based on an improved circular gabor filter and scale invariant feature transform. Sensors 2013;13(7):9248–66.
[9] Borah TR, Sarma KK, Talukdar P. Retina and fingerprint based biometric identification system. Int J Comput Appl (IJCA) 2013;74.
[10] Ortega M, Penedo MG, Rouco J, Barreira N, Carreira MJ. Retinal verification using a feature points-based biometric pattern. EURASIP J Adv Signal Process 2009;2009:1–13.
[11] Abdelwahed H, Hashim A, Hasan A. Segmentation approach for a noisy iris images based on hybrid techniques. Eng Technol J 2020;38(11):1684–91.
[12] Rapaka S, Kumar PR, Katta M, Lakshminarayana K, Kumar NB. A new segmentation method for non-ideal iris images using morphological reconstruction FCM based on improved DSA. SN Appl Sci 2021;3(1):1–15.
[13] Varkarakis V, Bazrafkan S, Corcoran P. Deep neural network and data augmentation methodology for off-axis iris segmentation in wearable headsets. Neural Networks 2020;121:101–21.
[14] Jan F, Min-Allah N. An effective iris segmentation scheme for noisy images. Biocyber Biomed Eng 2020;40 (3):1064–80.
[15] Hao K, Feng G, Ren Y, Zhang X. Iris segmentation using feature channel optimization for noisy environments. Cognitive Comput 2020;12(6):1205–16.
[16] Sahmoud, S. and Fathee, H.N., 2020, February. Fast Iris Segmentation Algorithm for Visible Wavelength Images Based on Multi-color Space. In International Conference on Advanced Concepts for Intelligent Vision Systems (pp. 239-250). Springer, Cham.
[17] Kheirolahy, R., Ebrahimnezhad, H. and Sedaaghi, M.H., 2009, October. Robust pupil boundary detection by optimized color mapping for iris recognition. In 2009 14th International CSI Computer Conference (pp. 170-175). IEEE.
[18] Lee S, Lee D, Park Y. Pupil segmentation using orientation fields, radial non-maximal suppression and elliptic approximation. Adv Elec Comput Eng 2019;19(2):69–74.
[19] Omran M, AlShemmary EN. An iris recognition system using deep convolutional neural network. J Phys Conf Ser 2020;1530 (1):012159. IOP Publishing.
[20] Şimşek İB, Şirolu C. Analysis of surgical outcome after upper eyelid surgery by computer vision algorithm using face and facial landmark detection. Graefe's Arch Clin Exp Ophthalmol 2021:1–7.
[21] Jalilian E, Karakaya M, Uhl A. CNN-based off-angle iris segmentation and recognition. IET Biom 2021;10(5):518–35.
[22] Jan F, Min-Allah N, Agha S, Usman I, Khan I. A robust iris localization scheme for the iris recognition. Multimedia Tools Appl 2021;80(3):4579–605.
[23] Sardar M, Banerjee S, Mitra S. Iris segmentation using interactive deep learning. IEEE Access 2020;8:219322–30.
[24] Jan F, Alrashed S, Min-Allah N. Iris segmentation for non-ideal Iris biometric systems. Multimedia Tools Appl 2021:1–29.
[25] Li YH, Huang PJ, Juan Y. An efficient and robust iris segmentation algorithm using deep learning. Mobile Inf Syst 2019;2019:1–14.
[26] Horn B, Klaus B, Horn P. Robot vision. MIT press; 1986.
[27] Faugeras O, Faugeras OA. Three-dimensional computer vision: a geometric viewpoint. MIT press; 1993.
[28] Hadwiger H. Minkowskische addition und subtraktion beliebiger punktmengen und die theoreme von Erhard Schmidt. Math Z 1950;53(3):210–8.
[29] Suzuki S. Topological structural analysis of digitized binary images by border following. Comput Vision Graph Image Process 1985;30(1):32–46.
[30] Sklansky J. Finding the convex hull of a simple polygon. Pattern Recogn Lett 1982;1(2):79–83.
[31] Otsu N. A threshold selection method from gray-level histograms. IEEE Trans Systems Man Cybernetics 1979;9 (1):62–6.
[32] Davies ER. Computer and machine vision: theory, algorithms, practicalities. Academic Press; 2012.
[33] Atherton TJ, Kerbyson DJ. Size invariant circle detection. Image Vis Comput 1999;17(11):795–803.
[34] Zhang C, Huber F, Knop M, Hamprecht FA. Yeast cell detection and segmentation in bright field microscopy. In: 2014 IEEE 11th International Symposium on Biomedical Imaging (ISBI). IEEE; 2014. p. 1267–70.
[35] Al-Sharadqah A, Chernov N. Error analysis for circle fitting algorithms. Electron J Statistics 2009;3:886–911.
[36] Tahir AA, Anghelus S. An accurate and fast method for eyelid detection. Int J Biometrics 2020;12(2):163–78.
[37] Ak TA, Steluta A. An iris recognition system using a new method of iris localization. Int J Open Inf Technol 2021;9 (7):67–76.
[38] Geem ZW, Kim JH, Loganathan GV. A new heuristic optimization algorithm: harmony search. Simulation 2001;76 (2):60–8.
[39] Nadia B, Abdessalam B, Mohamed B. Eyelids, eyelashes detection algorithm and houghtransform method for noise

removal in iris recognition. Indonesian J Elec Eng Comput Sci 2020;18:731–5.
[40] Liu CC, Chung PC, Lyu CM, Liu J, Yu SS. A novel iris segmentation scheme. Math Problems Eng 2014;2014:1–14.
[41] Horng MH. Performance evaluation of multiple classification of the ultrasonic supraspinatus images by using ML, RBFNN and SVM classifiers. Expert Syst Appl 2010;37(6):4146–55.